# Expanded View Figures

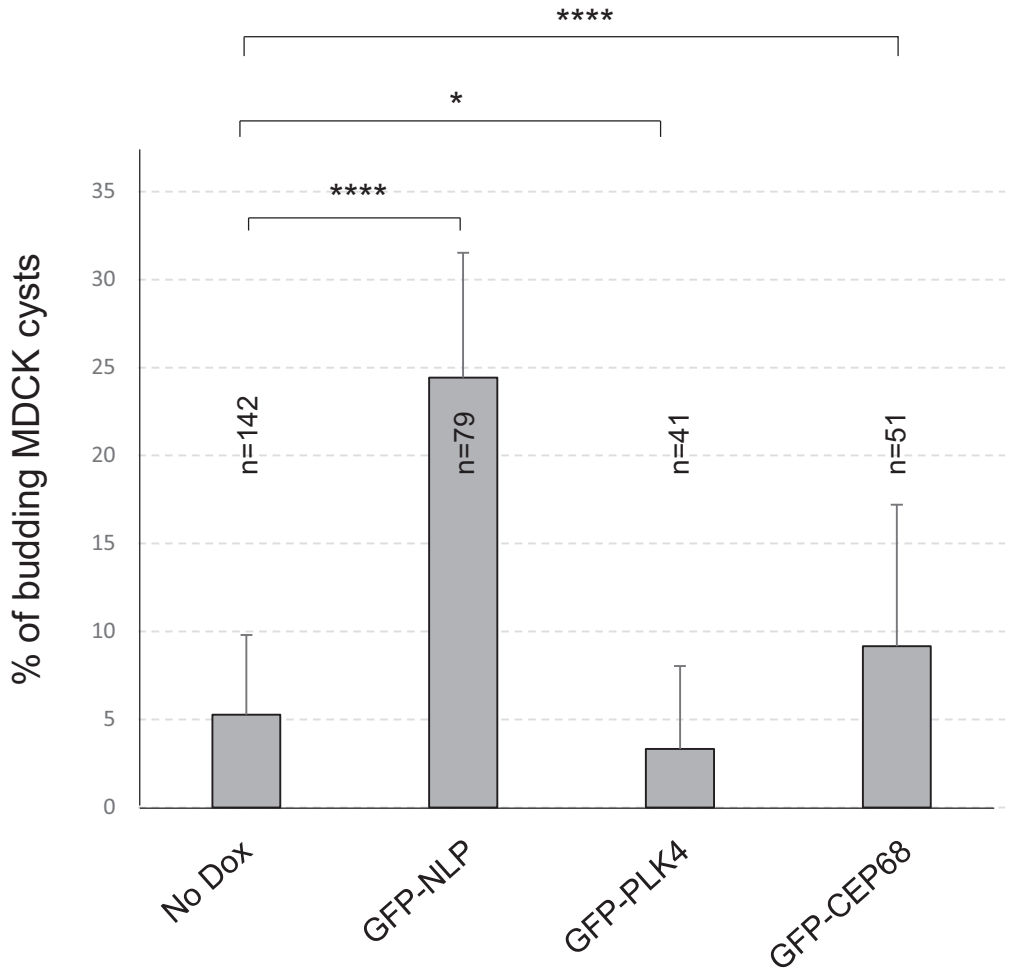


**Figure EV1. NLP overexpression induces budding in MDCK cysts.**

Histogram shows the proportions of MDCK cysts, cultured in pure Matrigel (without addition of collagen I), that exhibit budding after overexpression of GFP-NLP, GFP-PLK4, or GFP-CEP68, in comparison to non-induced acini (No Dox); error bars indicate + s.d. of the mean from three independent experiments, and *n* indicates the number of cysts analyzed from three independent experiments, *P*-values were derived from unpaired, two-tailed Student's *t*-test. ****$P < 0.0001$ and *$P < 0.05$, respectively.

**Figure EV2. Centrosome aberrations induce invadopodia formation in collagen I-enriched Matrigel.**

A, B Representative images showing invadopodia formation in response to overexpression of either GFP-PLK4 (A) or GFP-NLP (B) in MCF10A acini cultured in collagen I-enriched Matrigel. Acini were fixed and stained for α-tubulin (orange), F-actin (red), and DNA (blue); GFP-tagged transgene products are shown in green. Scale bars = 10 μm.

C Schematic description of experiments. Histogram shows quantification of the proportions of acini showing invadopodia formation in collagen I-enriched Matrigel; error bars indicate + s.d. of the mean from three independent experiments, and *n* indicates the number of acini analyzed. *P*-values were derived from unpaired, two-tailed Student's *t*-test. *$P < 0.05$.

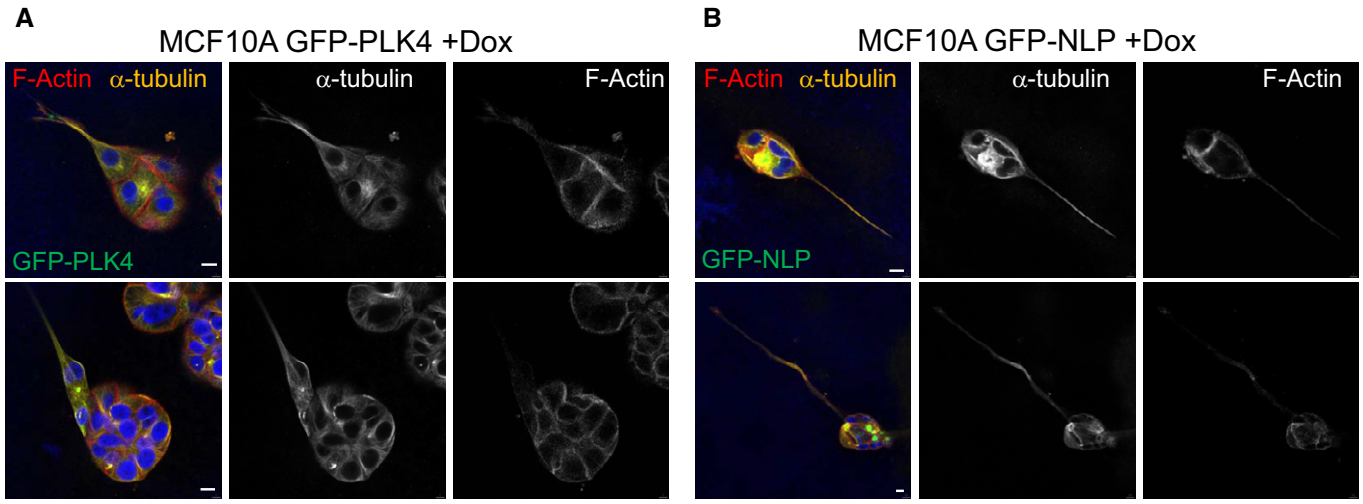


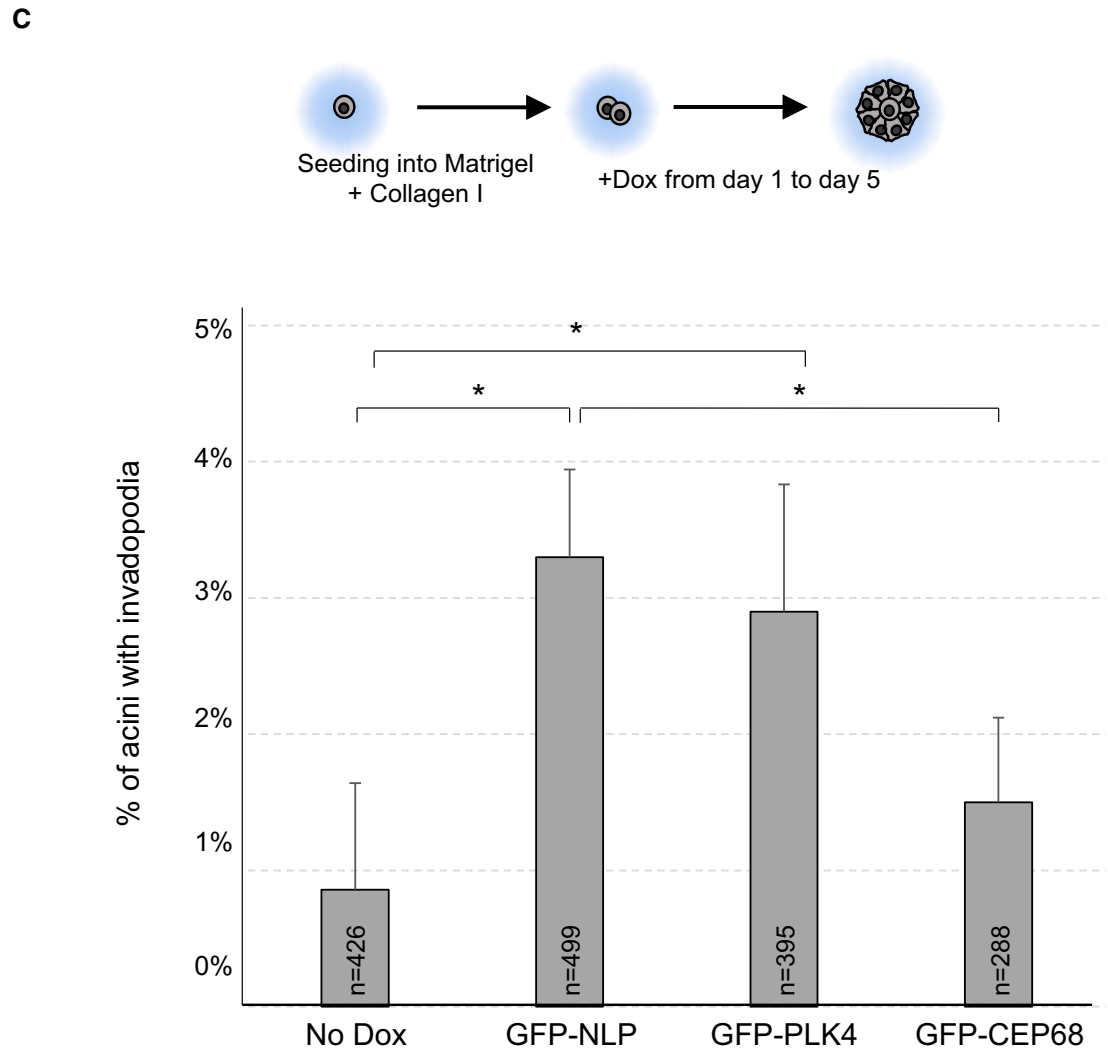


**Figure EV2.**

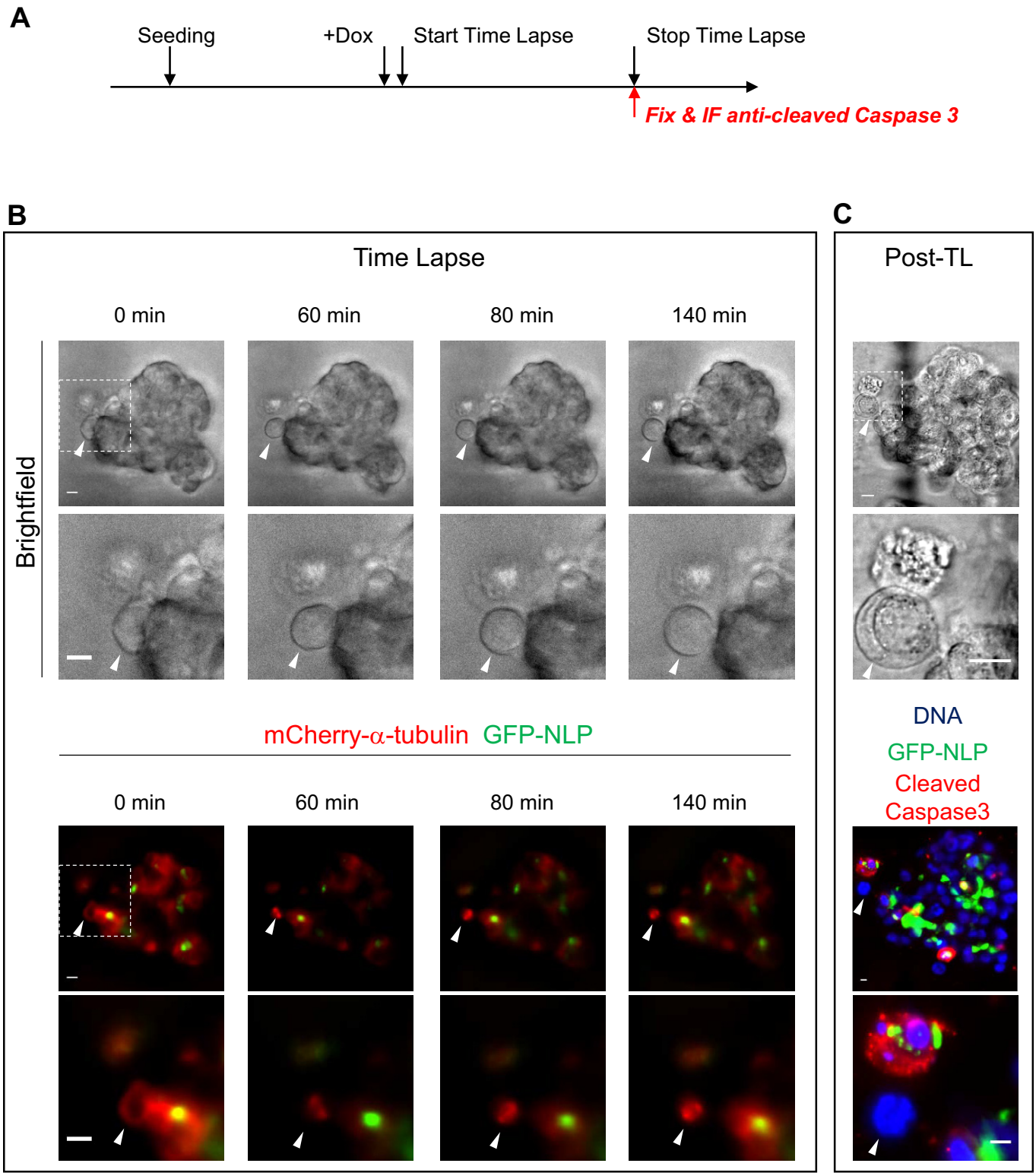


**Figure EV3.**

**Figure EV3. A proportion of budding mitotic cells are negative for cleaved caspase 3.**

A Schematic description of experiments.

B Still series from time-lapse experiments showing mitotic cell budding from MCF10A acini overexpressing GFP-NLP; shown are bright field images (upper panels) and fluorescence images (lower panels) allowing detection of mCherry-α-tubulin (red) and GFP-NLP (green). Dashed squares represent the regions chosen for enlargements that are shown below each bright field and fluorescence image. White arrowheads point to budding cells. Images were acquired every 20 min and time stamps are indicated. Scale bars = 10 μm.

C At the end of time-lapse imaging, acini were fixed and processed for immunofluorescence using antibodies against cleaved caspase 3 to detect apoptotic cells. Previously recorded acini were identified through use of a gridded area and white arrowheads point to the budding cells that had been monitored. Immunofluorescence images show DNA (blue) GFP-NLP (green) and cleaved caspase 3 (red). Scale bars = 10 μm.

**Figure EV4. Impact of cell cycle and cytoskeleton on stiffness of 2D MDCK cells.**

A Exemplary stiffness histograms of MDCK cells (such as in Fig 6A), comparing GFP-NLP$^-$ cells (top) and GFP-NLP$^+$ MDCK cells (bottom) in the same 2D culture. Counts report the number of force curves per bin. (Insets) Corresponding stiffness maps show cells (marked by green lines) for GFP-NLP$^-$ cells (top) and GFP-NLP$^+$ cells (bottom) in the same 2D culture. Note the increased stiffness of the GFP-NLP$^+$ cells (peak shift to the right), as illustrated by the dotted lines.

B Confocal microscopy experiments visualize drug-induced changes in the actin and microtubule cytoskeletons of GFP-NLP$^+$ cells; shown are confocal slices with top views (xy; main panels) and lateral views (xz, lower panels, and yz, right hand panels). Thin white lines refer to the positions of the optical sections. Scale bars = 5 μm.

C Single (non-confluent) wild-type MDCK cells are depicted in the bright field signal with the AFM probe located in proximity (left). Interphase cells (top) are differentiated from mitotic cells (bottom) that show a positive epifluorescence signal for mCardinal-H1 (right). Bright field and epifluorescence images are 90 × 45 μm.

D Stiffness of single MDCK cells in interphase or mitosis. Note that mitotic cells are significantly stiffer than interphase cells. All box plots show the mean (square) and median (line); the whiskers are s.d., and the box is s.e.m. The statistical significance was tested using a Mann–Whitney test. *$P < 0.05$.

E Upper row shows representative maps of quasi topography (left), cellular stiffness (middle), and the quasitopography/stiffness overlay (right) of interphase single cells; scale bars = 10 μm. Lower row shows representative maps of quasi topography (left), stiffness (middle), and the quasitopography/stiffness overlay (right) of isolated mitotic cell; scale bars = 2 μm. Note that analyzed areas were limited to the top of the mitotic cells (ca. 25 μm$^2$) to ensure correct measurements and avoid any bias caused by the increase of cortex curvature induced by mitotic rounding. Scale bars = 10 μm (upper panels); 2 μm (lower panels).

F Representative loading (forward/FWD, black dashed lines) and unloading (backward/BWD, red dashed lines) force curves highlight differences in the elastic and viscous regimes for single (left) versus confluent (right) cells in mitosis (Mitotic) or in interphase (Inter.). Individual mitotic MDCK cells are purely elastic whereas mitotic cells in confluency tend to be more viscous.

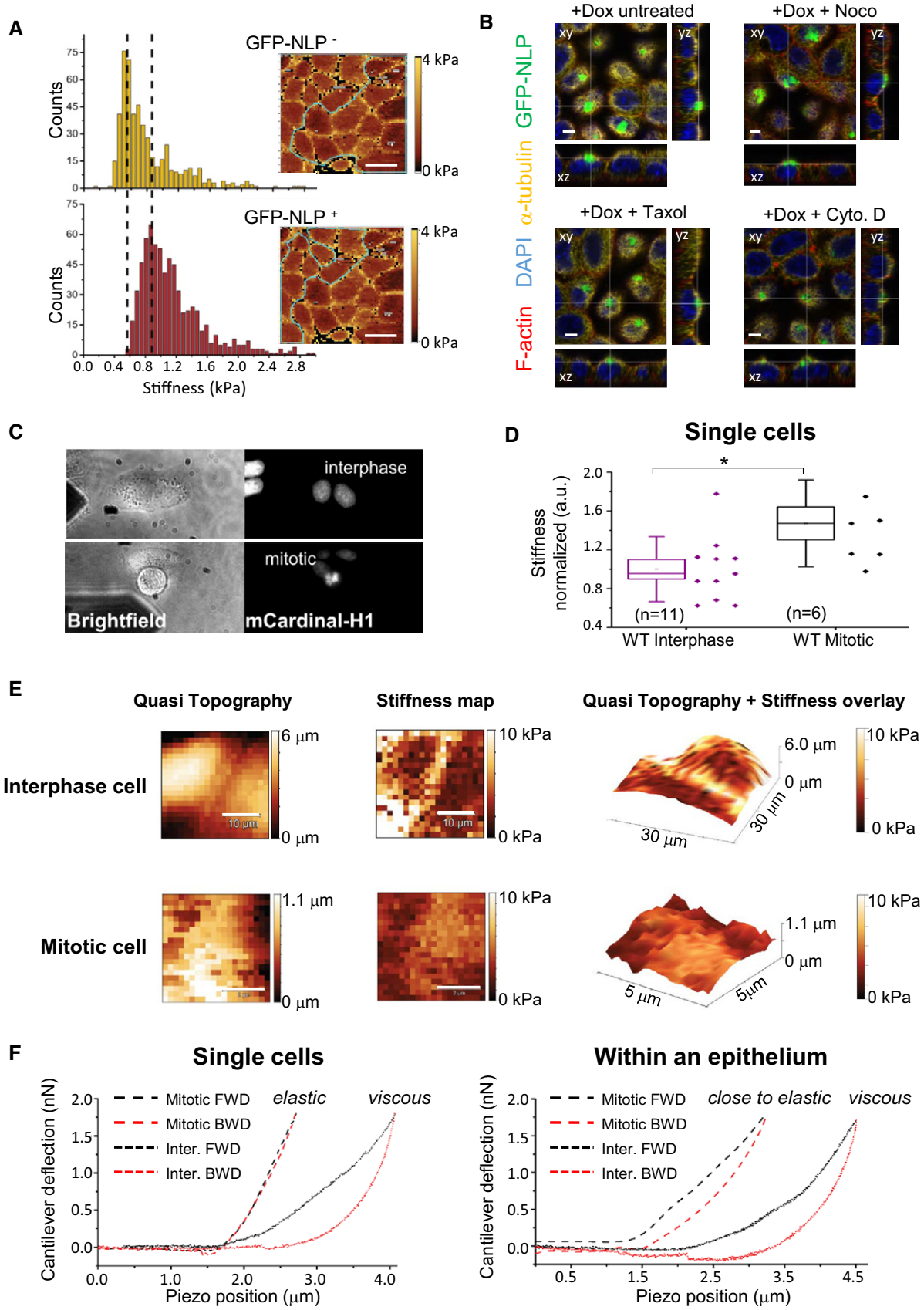


**Figure EV4.**

 

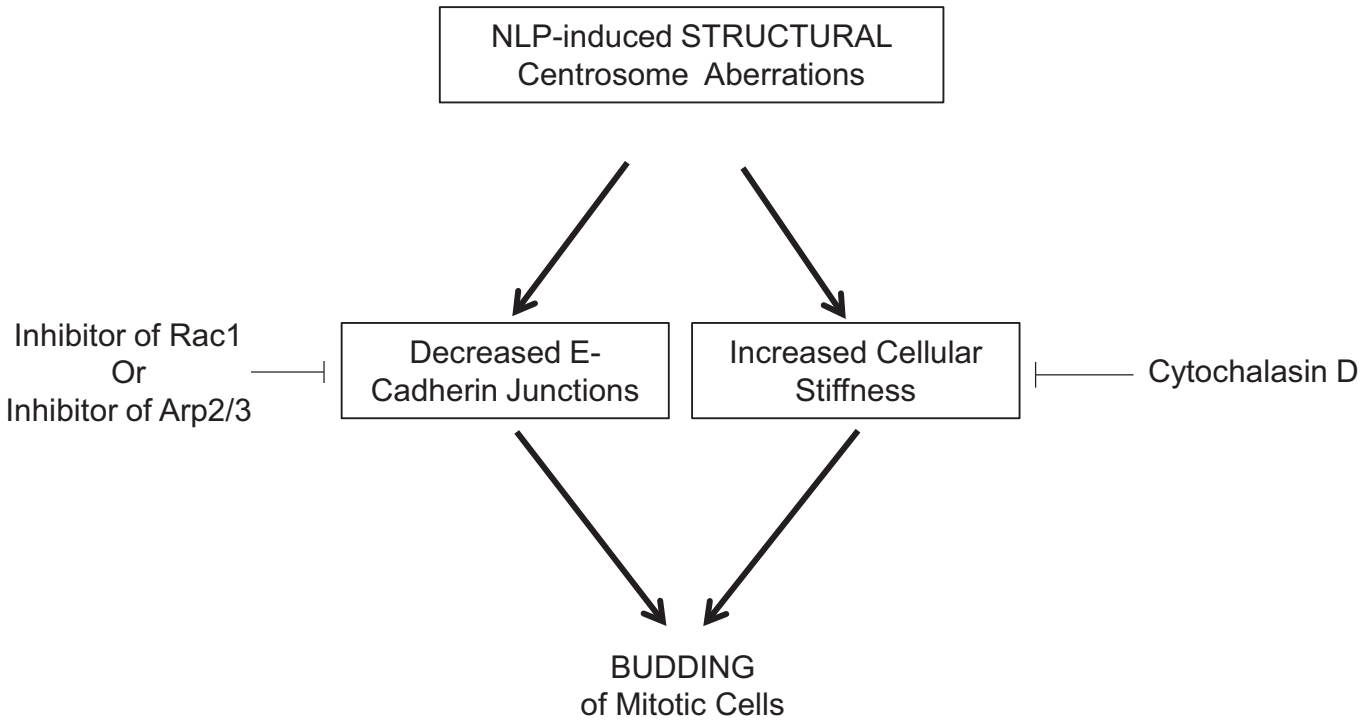


**Figure EV5. Structural centrosome aberrations trigger budding of mitotic cells through decreasing E-cadherin junctions and increasing cellular stiffness.**

Scheme shows that NLP-induced structural centrosome aberrations favor budding of mitotic cells through two distinct pathways that are both necessary but not sufficient. On the one side, NLP-induced centrosome aberrations induce a decreased of E-cadherin junctions that can be rescued by partial inhibition of the Rac1 or Arp2/3 activities, which consequently prevents budding. On the other side, budding also requires an increased of cellular stiffness that can be restored by depolymerizing the actin network by a cytochalasin D treatment. Such a treatment can also prevent budding induced by NLP overexpression.